Progress In Electromagnetics Research C, Vol. 119, 219–233, 2022

A Flower Shaped Miniaturized 4×4 MIMO Antenna for UWB Applications Using Characteristic Mode Analysis

Ankireddy C. Suresh* and Thatiparthi Sreenivasulu Reddy

Abstract—A novel design of a 4×4 miniaturized UWB-MIMO (multiple-input, multiple-output) antenna with isolation improvement is proposed in this paper. The designing procedure of a flower-shaped MIMO antenna is done using characteristic mode analysis (CMA). The flower-shaped UWB-MIMO antenna is made up of four symmetrical flower-shaped radiating elements that are isolated using an orthogonal method. The flower antenna's dimensions are $40 \times 40 \times 1.6\,\text{mm}^3$ ($0.44\lambda_0 \times 0.44\lambda_0 \times 0.017\lambda_0$). A flower-shaped radiator is used to get good the isolation in MIMO elements. Further isolation is enhanced by inserting a swastik-shaped stub on the ground to get return losses of $S_{11} < -10\,\text{dB}$ and isolation of $S_{12} < -18\,\text{dB}$. The designed antenna covers the entire UWB (3.1 GHz–14 GHz) spectrum for impedance matching, including (10.7 GHz to 11.7 GHz), 11 GHz (10.7 GHz to 11.7 GHz), and 13 GHz (10.7 GHz to 11.7 GHz) (12.75 to 13.25 GHz). Good diversity performance is achieved in the UWB and ITU range. The designed antenna has a gain of 5.5 dB, an efficiency of 89%, an impedance bandwidth of 123.61%, an envelope correlation coefficient of 0.012, a diversity gain of nearer to 10 dB, a capacity channel loss of 0.29 bp/s/Hz, and a mean effective gain of less than $-3.1\,\text{dB}$. The designed antenna is fabricated and tested. These simulated results are validated in state-of-the-art laboratories. According to the simulation and measurement results, this antenna is well suited for reliable wireless communication systems. The potentiality of the designed antenna is high, and the antenna is compact and portable.

1. INTRODUCTION

In 2002, the Federal Communications Commission recognized ultra-wideband (UWB) technology and assigned the unlicensed frequency spectrum (3.1 GHz–10.6 GHz) to it. This frequency range was chosen for a variety of commercial and mobile applications [1]. UWB is a promising technology that provides increased bandwidth and high-speed data transmission links. UWB technology is limited to a short range and low data rates due to its low power spectral density. Due to its low power capabilities, UWB also had issues with multipath and fading. By combining UWB technology with multiple-input and multiple-output (MIMO), the bottleneck problem of UWB can be solved. The spatial multiplexing-gain is the solution for UWB [2]. The combination of UWB and MIMO in wireless communication systems allows for higher data rates and greater reliability. The number of antennas in a UWB communication system is determined by the channel capacity of the system. When the number of antennas in a system is increased, the channel capacity increases as well. Because the transmitted power is constant, choose the most appropriate antenna array to maximize channel capacity [3]. However, cramming more antenna elements into a small space boosts mutual interaction. The MIMO's performance suffers as a result. The processes listed below are used to reduce mutual interference. 1. Faulty Ground Structure (DGS). 2. EMG stands for Electromagnetic Band Gap. 3. Network decoupling. 4. Parasite elements. 5. Neutralization lines [4–20] metamaterial. Because of the bottleneck problem of UWB power limits, antenna designers have focused on MIMO systems combining UWB and other technologies. Antenna

Received 2 February 2022, Accepted 22 March 2022, Scheduled 10 April 2022
* Corresponding author: Ankireddy Chandra Suresh (archandu.suresh@gmail.com).
The authors are with the Department of Electronics and Communication Engineering, SVUCE, SV University, Tirupathi, A.P, India.

designers should keep an eye on rapid changes in wireless communication systems that require a lot of bandwidth, such as the internet of things (IoT). The International Telecommunication Union (ITU) has recommended the frequency bands 11 GHz (10.7 GHz–11.7 GHz) and 13 GHz (12.75–13.25 GHz) for complex electronic wireless systems to meet the demand for large bandwidth in IoT and internet-based electronic devices [17, 18]. Beyond the UWB range, researchers have begun work. The 2×2 UWB-MIMO antenna uses a decoupling structure to achieve greater than 31 dB isolation, but the antenna is not portable due to its size of $93 \times 47 \times 1.6\,\text{mm}^3$ [4]. The high isolation and large bandwidth between 1.99 GHz and 10.02 GHz were achieved using two identical semi-circular radiating elements with a symmetrical stepped elliptical structure and an I-shaped ground structure [5]. Two symmetrical co-radiators are shared by a pentagonal radiator (MIMO). A T-shaped slot on the radiator and a stub on the ground plane provide excellent isolation [6]. Individual radiating elements in 2×2 MIMO are separated by 90° angularly, with a stepped structure that improves isolation. The use of defected ground compact electromagnetic band gap (DG-CEBG) improves further isolation ($S_{21} < -18\,\text{dB}$) [7]. To reduce the length of an 8-port (3-dimensions) UWB MIMO antenna, 1–4 elements are arranged perpendicular to 5–8 elements. Stubs of inductor capacitor (LC) are arranged on ground to start reducing mutual interference ($S_{21} < -17\,\text{dB}$) among the elements. To achieve good radiation characteristics, this antenna used space diversity and polarization diversity techniques. This antenna is well suited for WLAN [8]. Four radiating elements are placed orthogonally in a 4×4 UWB MIMO antenna, and each radiator is activated by an LC stub along the ground plane via a PIN diode. The radiators are placed orthogonally to each other to achieve high isolation and impedance bandwidth [9]. By arranging four radiators in a planner configuration and remaining four radiators perpendicular to the planner structure, an 8-element MIMO antenna with dimensions of $50 \times 50 \times 25\,\text{mm}^3$ (3-Dimension) is created. The polarization diversity technique is used to achieve a high degree of isolation of more than 17 dB as well as a wide impedance bandwidth over a wide frequency spectrum. To attain greater isolation and impedance bandwidth, the radiators are positioned orthogonally to one another [10]. Each element of a 2×2 MIMO antenna is designed as a modified square patch radiator. This antenna can be reconfigured by aligning the elements orthogonally to the antenna's corner, resulting in a high degree of isolation of more than 20 dB [11]. The pentagonal 4×4 radiators are arranged orthogonally to each other and have a rectangular slot on each element to achieve a high isolation of greater than 32 dB [12]. To achieve good isolation, a 4×4 UWB-MIMO antenna ($48 \times 34 \times 1.6\,\text{mm}^3$) with a neutralization technique is used, which further improves the efficiency of the radiation to 79.9%; the gain is 2.91 dB; the bandwidth is 96.4%; and the diversity gain is about 10 dB [13]. Using the loop excitation method, a Yagi-based 2×2 UWB-MIMO is designed in which half-driven loop method is employed to reduce the antenna's length up to 45%. They also achieved high isolation of up to 17 dB, gain of 6 dB, and an ECC of less than 0.0568 [14]. Each of the four radiators in a planar quad element wide band MIMO antenna is partially grounded and loaded with a splint ring resonator (SRR). This WiMAX antenna has a peak gain of 4 dB and a high isolation of more than 15 dB. The peak efficiency is 91.1%, and the overall size is very small [15]. Four symmetrical circle-shaped radiators are placed on a partially slotted ground for high isolation in this 4×4 MIMO antenna. Across the entire UWB frequency spectrum (3.1 GHz–10.6 GHz), this antenna arrangement provides isolation of up to 20 dB. The average gain is 3.28 dBi, and the ECC is less than 0.002 [16]. All elements in the 4×4 MIMO antenna are tried to arrange orthogonally to obtain −20 dB isolation, and each radiating element has a C-shaped slot. Across the entire UWB spectrum (3.1 GHz–10.6 GHz), the diversity properties are satisfactory [17]. To achieve a 20 dB isolation in a 2×2 MIMO antenna, F-shaped stubs are used. This antenna has 20 dB isolation, an ECC of 0.04, and a diversity gain (DG) of more than 7.4 dB [18]. Two U-shaped elements and two circular elements are organized orthogonally to each other to improve the diversity characteristics of the 4 UWB-MIMO antennas. This antenna has 17 dB isolation [19]. The electronically reconfigurable MIMO antenna is built for high isolation and uses decoupling networks to show band notch characteristics [20]. To achieve high isolation, an L-shaped radiator is etched with an ohm symbol, and various metasurface absorber low RCS networks are used [21–23].

All of the antenna designs listed above are only good in certain antenna parameters. The mutual coupling in MIMO will increase if a large number of ports are gathered in a small area. A complex decoupling structure is used to reduce mutual interference. The complex decoupling structures affect the radiation performance as well as reducing mutual coupling. Some antenna designs provide more

bandwidth at the expense of isolation. Because of lack of a systematic and sophisticated design process, the antenna designers were unable to meet the good diversity performance metrics. The CMA method is a systematic design method. The requirements of UWB wireless communications will be met by applying CMA in a step-by-step process. We can use the CMA to learn more about the physical structure of the antennas.

The trial and error method of antenna design wastes a significant amount of time. The CMA uses a systematic design approach to minimize time waste while designing antennas. The proposed flower-shaped 4×4 UWB-MIMO antenna has a bandwidth of more than 11 GHz, which includes both UWB and ITU bands. To meet the goals of the UWB applications, the designed antenna is implemented using CMA. The antenna is made up of four flower-shaped radiators that are devoid of petals. This proposed antenna is designed to meet ECC, DG, CCl, and MEG diversity requirements.

2. DESIGN OF FLOWER-SHAPED 4×4 UWB-MIMO

Four symmetrical flower-shaped radiators that are orthogonal to each other make up the 4×4 miniaturized UWB-MIMO design. To reduce mutual interference, this antenna employs the space diversity technique [24]. The flower-shaped radiator is made up of two different-sized flowers arranged in a flower shape. This flower radiator lacks petals and has sepals. As depicted in Fig. 1, the overall dimensions of the 4×4 miniaturized UWB-MIMO antenna are $(0.44\lambda_0 \times 0.44\lambda_0 \times 0.017\lambda_0)$ $(40 \times 40 \times 1.6\,\text{mm}^3)$ designed on an FR-4 substrate, with $\tan\delta = 0.002$ and $\varepsilon r = 4.3$.

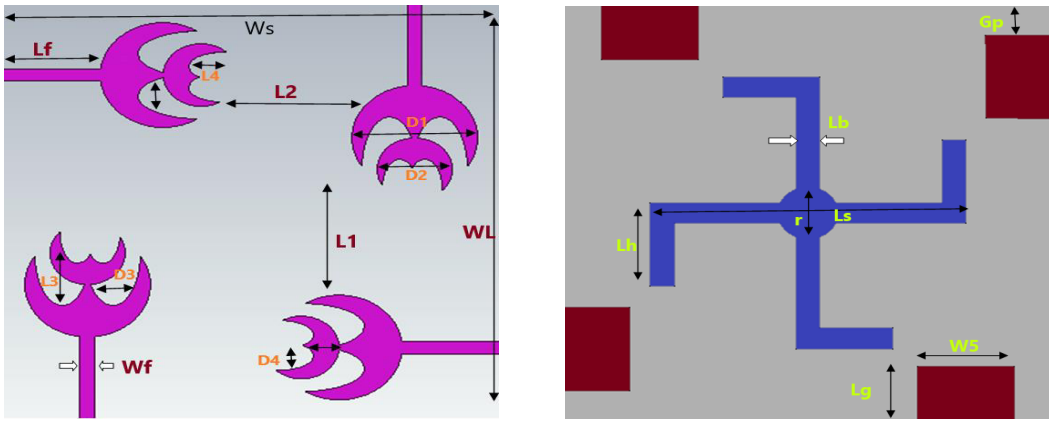

(a) (b)

Figure 1. The dimensions of the proposed 4×4 flower-shaped UWB MIMO antenna. (a) Top view. (b) Bottom view.

Design procedure to make flower radiator: 1) Consider a new circular patch with a radius 5 mm. 2) Remove some top and bottom portions of the circular patch to differentiate petals and sepals. 3) Repeat step 2, to make flower radiator provide desired impedance bandwidth (3.1 GHz–13.75 GHz), gain, and efficiency. The absence of petals in a flower radiator increases low-frequency isolation. The single radiator has two flowers, each with a diameter of 10 mm for the lower flower sepal and 5 mm for the upper flower sepal. Etchings in the shape of petals measure 4.4 mm and 2.8 mm in the upper flower and lower flower, respectively, on this flower radiator. In Fig. 1(a), orthogonal radiators are separated by 9 mm. The ground plane is made up of four ground edges, each of which is rectangular in shape and measures $5.375 \times 8\,\text{mm}^2$ in length and width. By using the parametric study of single flower-shaped radiator, reflection coefficient and isolation among the elements are analyzed. Firstly analyze the reflection coefficient of single radiator by changing the length of the ground (Lg) from 3 mm to 7 mm. The corresponding S_{11}-parameters, and isolation are depicted in Fig. 2(a) & Fig. 2(b). Repeat the same procedure by varying the values of diameter of petal ($D3$), height of the higher petal ($L4$), and depict its corresponding reflections coefficients in Fig. 2(c) & Fig. 2(d). Place a 2.5-mm-radius

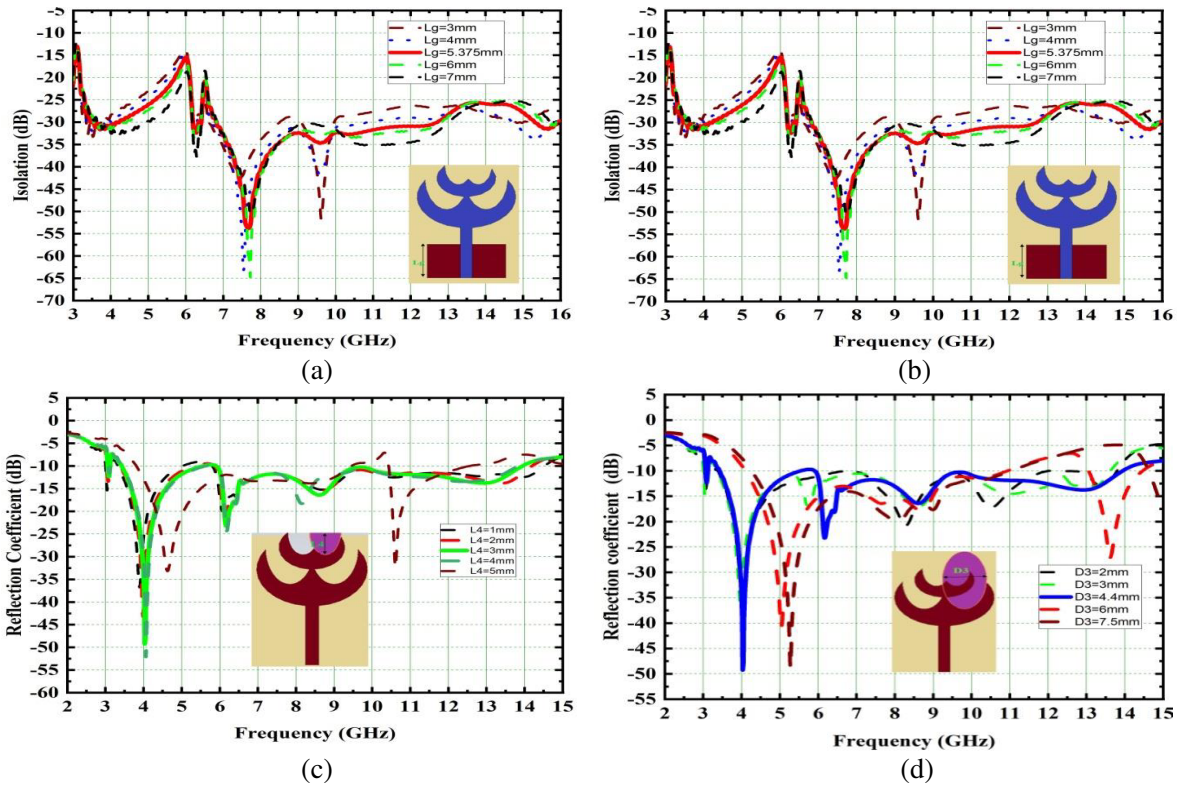

Figure 2. Parametric variations of single flower radiator w.r.t.. (a) Length of the ground Lg. (b) Isolation due to Lg. (c) Variations in $L4$ (height of the Upper Petal). (d) Variations in $D3$ (Diameter of the lower petal).

circular patch in the ground plane's center to improve isolation. This antenna generates good isolation in the UWB (3.1 GHz–10.6 GHz) range only using the considered ground plane arrangement. Impedance bandwidth in the ITU band is enhanced by combining two S-shaped swasthik patches in the ground. This antenna configuration provides isolation between 3.1 GHz and 13.75 GHz, including the ITU band. Table 1 shows the dimensions of the 4×4 miniaturized flower-shaped antenna.

Table 1. The parameters of flower shaped antenna.

Parameters	Value (mm)	Parameters	Value (mm)
Length of the Substrate (WL)	40	Width of the Substrate (Ws)	40
Width of the Ground (Ls)	1.6	Width of S-Shaped Stub (Lb)	3
Diameter of the lower sepal ($d1$)	10	Length of the Feed (Lf)	9
Diameter of the Upper Sepal ($d2$)	6	Radius of the Ground Patch (r)	2.5
Diameter of lower petals ($d3$)	4.4	Height of the Ground S-Shaped Stub (Lh)	8
Diameter of Upper petals ($d4$)	2.8	Gap of the Ground patch (Gp)	1.5
Height of the Lower Petal ($L3$)	5	Distance b/w two radiators horizontally ($L2$)	9
Height of the Upper Petal ($L4$)	2	Length of the S-Shaped Patch (Ls)	26
Distance b/w two radiators vertically ($L1$)	9	Width of Feed (Wf)	1.2
Width of the ground patch ($W5$)	8	Length of the ground (Lg)	5.375

In four stages, the flower-shaped 4×4 miniaturized UWB-MIMO is studied: antenna0(A#0), antenna1(A#1), antenna2(A#2), and antenna3(A#3). Characteristic mode analysis is used to design the proposed 4×4 UWB-MIMO antenna. CMA analyzes the design process using performance metrics such as eigenvector, characteristic angle, and modal significance. The antenna is designed in CMA, and its performance is measured in characteristic mode currents. The mode current distributions in the CMA are observed without the use of feed and excitation. The impedance bandwidth along MIMO performance matrices is improved in the CMA method using this step-by-step systematic design approach. CMA designed the flower-shaped 4×4 UWB-MIMO using the Computer Simulation Tool (CST Ver.2018). A multi-layer solver or an integration equation solver is used to observe the mode current distribution in CST. Fig. 3 depicts the design and evaluation process.

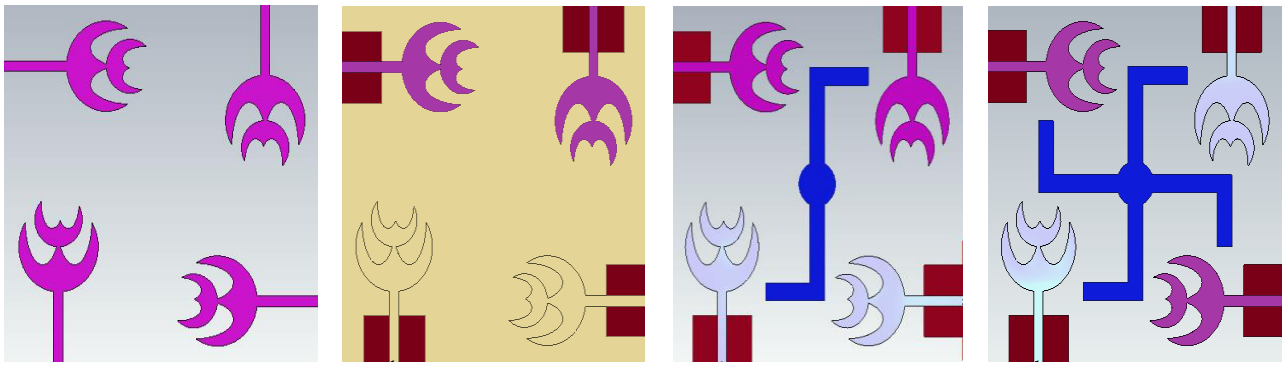

Figure 3. Evolution of 4×4 flower shaped antenna. (a) A#0. (b) A#1. (c) A#2. (d) A#3.

In CMA, matrices such as modal significance, characteristic angle, and eigenvalues are used to design antennas. The modal significance of this UWB-MIMO antenna was taken into consideration when the antenna is desinged [25]. An antenna's overall design is completed in four stages: A#0, A#1, A#2, and A#3 without the use of any feed or excitation [26]. To begin, A#0 is made up of four flower-shaped radiators, each with two flowers stacked one on top of the other. A#0's characteristic modes were investigated in the absence of excitation because it lacked a ground. To analyze physical insight into an antenna's structure, the design process generates ten characteristic modes. The modal significance of A#0 is depicted in Fig. 4(a). Nine of the ten characteristic modes (CMs) resonate between 4 GHz and 5 GHz, with the exception of mode 6. CM6 has a resonant frequency at 6.3 GHz. As a result, at low and high frequencies, none of the ten modes contribute any bandwidth or isolation. At low and high frequencies, the isolation is inadequate. There are only a few frequencies where all of the CMs are concentrated, and the corresponding modal significances are depicted in Fig. 4(a). The modes of modal significance for the remaining antennas, A#1, A#2, and A#3, are also analyzed and shown in Fig. 4. By applying feeding and excitation to the same four antennas, A#0, A#1, A#2, and A#3, time-domain analysis is performed [27]. Fig. 5 shows the relative S-parameters. The characteristic mode currents (CMCs) change their direction as the antenna design process progresses, depending on the isolation methods used. For CM3, the change in CMC direction of the 4×4 antenna is depicted in Fig. 6. Each mode has a modal significance, eigenvalue, and characteristic angle in characteristic mode theory, which are represented by matrices of characteristic mode analysis. Each metric has its own meaning, but they all represent the same features of a particular characteristic mode [28, 29].

All of the useful modes are useful in A#0, but lower and higher frequencies are not covered. That is to say, this A#0 is bad at low frequencies and high frequencies, and excellent at mid-band frequencies (4 GHz–6 GHz).

In UWB, A#0 has low isolation and high mutual coupling among the radiators at both low and high frequencies. Because A#0 appears to lack a ground plane, there is more interaction between the radiating elements, resulting in high mutual coupling. We can deduce from A#0's S-parameters that A#0 has low isolation at low and high frequencies. A#1 has a partial ground plane at each radiator,

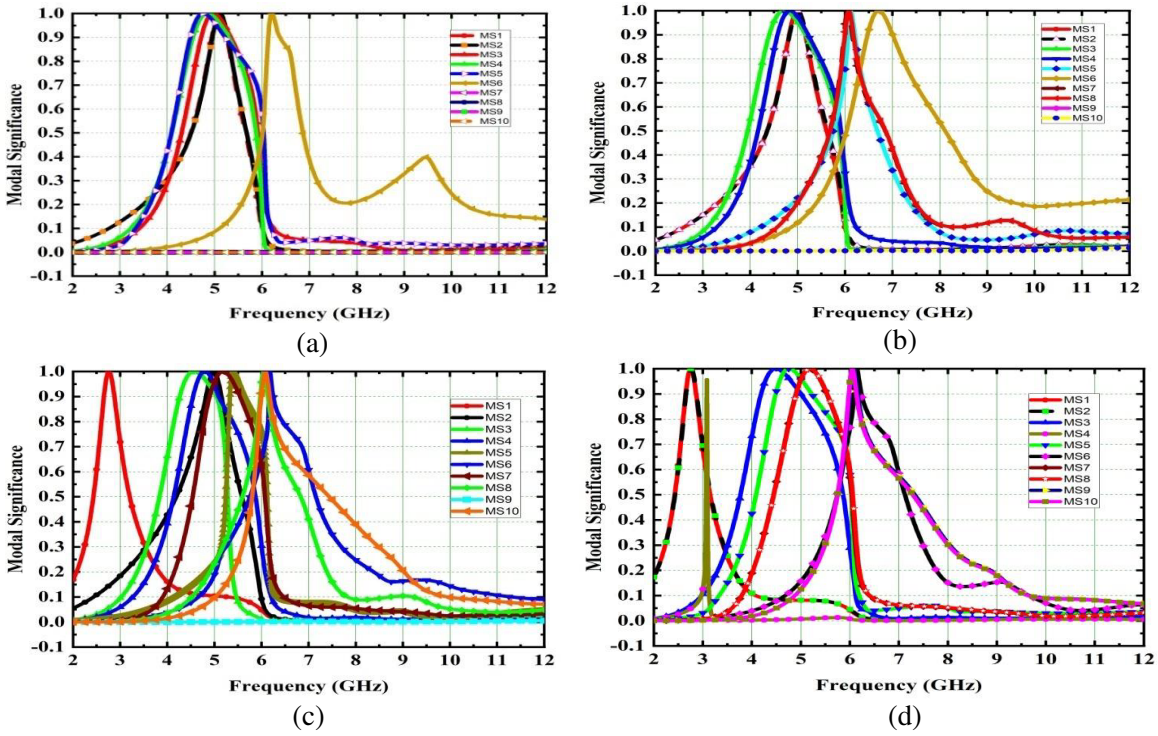

Figure 4. The modal significance of flower-shaped antenna. (a) A#0. (b) A#1. (c) A#2. (d) A#3.

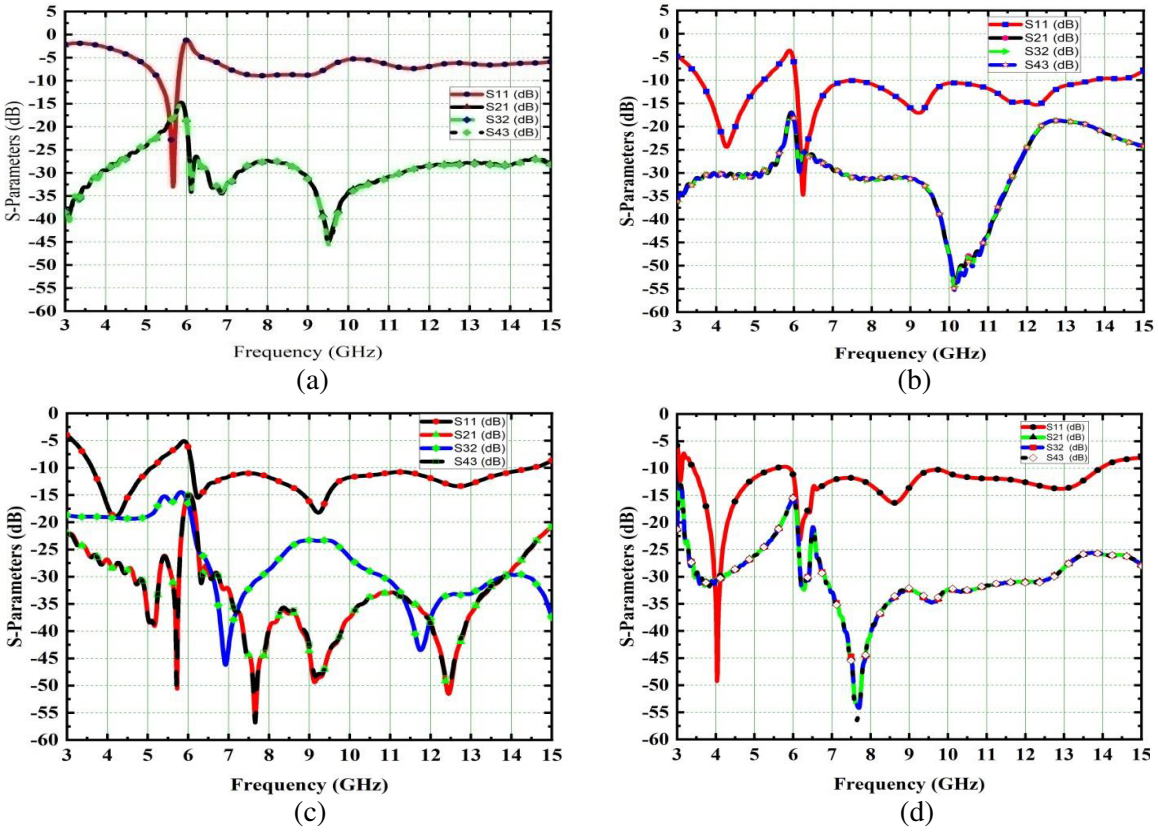

Figure 5. The S-parameter of flower-shaped antenna. (a) A#0. (b) A#1. (c) A#2. (d) A#3.

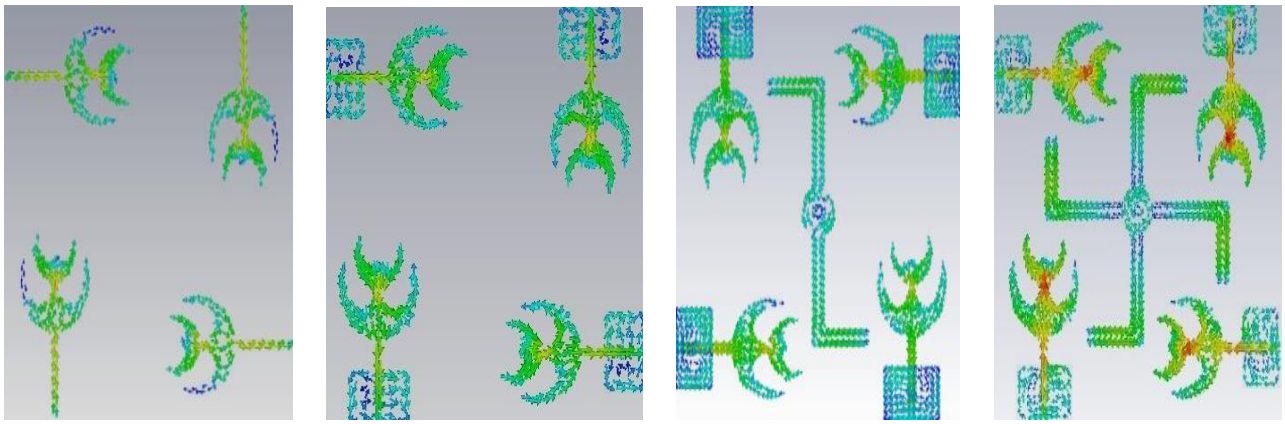

Figure 6. The fundamental CM current effect in the evolution of flower shaped antenna.

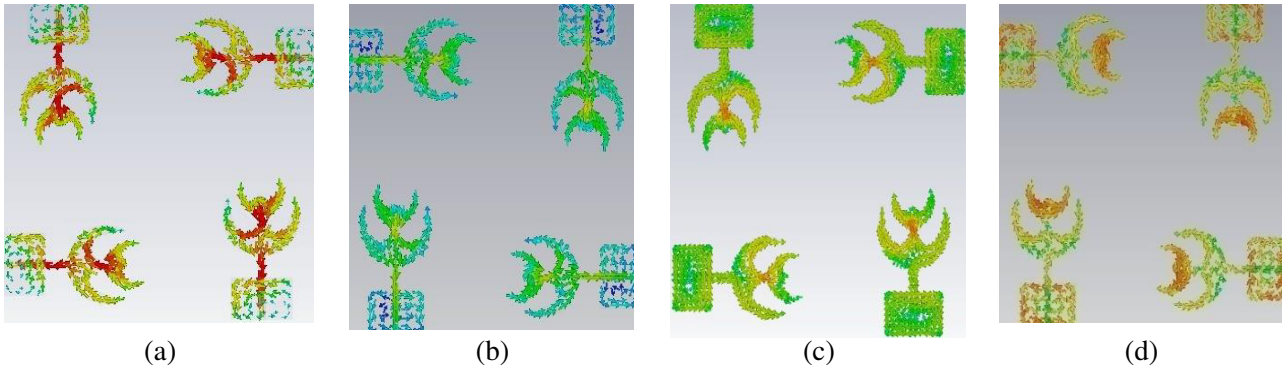

Figure 7. The characteristic currents of CM3 in A#1 at (a) 2.8 GHz, (b) 4.1 GHz, (c) 6.2 GHz, and (d) 8.6 GHz.

and its current distributions in the UWB spectrum at different frequencies are seen in Fig. 7. There are four stages to the evolution of a flower-shaped antenna design. Adjusting the CMs in the low and high frequency regions can achieve a wideband frequency response. A#1 is the next stage after A#0. Along with A#0, A#1 has a ground plane. On the ground plane, each radiator is given a $5.375 \times 8\,\text{mm}^2$ ground patch. With the exception of CM3, CM9, and CM10, all modes shifted to the mid-band and high frequencies. The contributions of CM9 and CM10 were negligible. The location frequency of the CM3 did not change. As a result, the current interaction among the elements is reduced in this antenna design, resulting in less interference. Fig. 4(b) shows the modal significance of A#1. The corresponding A#1 S-parameters are shown in Fig. 5(b). A#1 has a partial ground, and its current distributions are shown in Fig. 7. At mid-frequencies, the current densities and distributions are extremely strong. However, because the majority of the modes are concentrated at mid-frequencies, they still require low-frequency isolation. As a result, there is a good chance that radiating elements will come into contact with the current.

2.1. Effect of Swastik Shaped Ground

An S-shaped ground is added to A#1 to form A#2 in this antenna design. An S-shaped stub is added to reduce additional mutual coupling. In the centre of the ground plane, an S-shape stub with a width of 3 mm and a length of 26 mm is placed, as shown in Fig. 3(c). A 2.5 mm-circular radius patch and an S-shaped stub are added to the ground patch's centre. Without using feed or excitation, look at

A#2 in characteristic modes. Except for CM3, CM9, and CM10, some modes are moved to the low frequency band and some modes moved to the mid-band frequency region due to the placement of a novel shaped S-stub in the ground. However, CM3 remains unchanged and resonates at 5 GHz. Fig. 4(c) depicts the corresponding modal significance. Mutual coupling was reduced slightly in A#2 because current distributions are formed between the ground plane and radiators. Fig. 8 depicts the current distributions in A#2 at various frequencies. Using feed and excitation, the same A#2 is now analyzed in time-domain analysis. Fig. 5(c) shows the corresponding S-parameters. In A#3 antenna, the vertical S-shaped stub added with a horizontal S-shaped stub to form a swastik-shaped stub on the ground plane. Some modes, such as CM1, CM2, and CM4, are moved to the low frequency region by placing a swastik shape stub on the ground plane, which contributes to good isolation at low frequencies. The modes CM3, CM5, and CM6 are concentrated at mid-band frequencies and provide good isolation there, as CM7 and CM8 contribute to isolation at high-band frequencies in the UWB spectrum. However, because mode CM3 did not move as a result of the placement of stubs, it is known as the dominant mode. Fig. 4(d) depicts the respective modal significances. In Fig. 5(d), the respective S-parameters of A#3 are shown.

Including a swastik shape stub in the ground plane improves isolation and results in good MIMO antenna performance metrics. Figs. 9 and 10 depict the A#3 characteristics of currents and current densities at various frequencies.

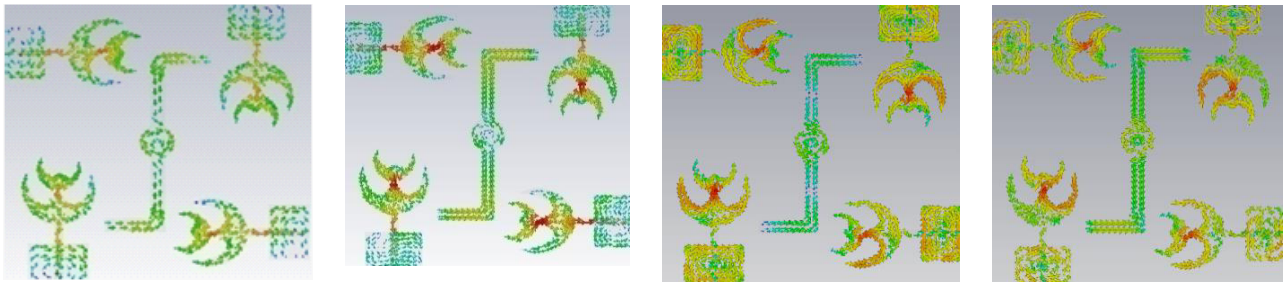

Figure 8. The characteristic currents of CM3 in A#2 at (a) 2.8 GHz, (b) 4.1 GHz, (c) 6.2 GHz, and (d) 8.6 GHz.

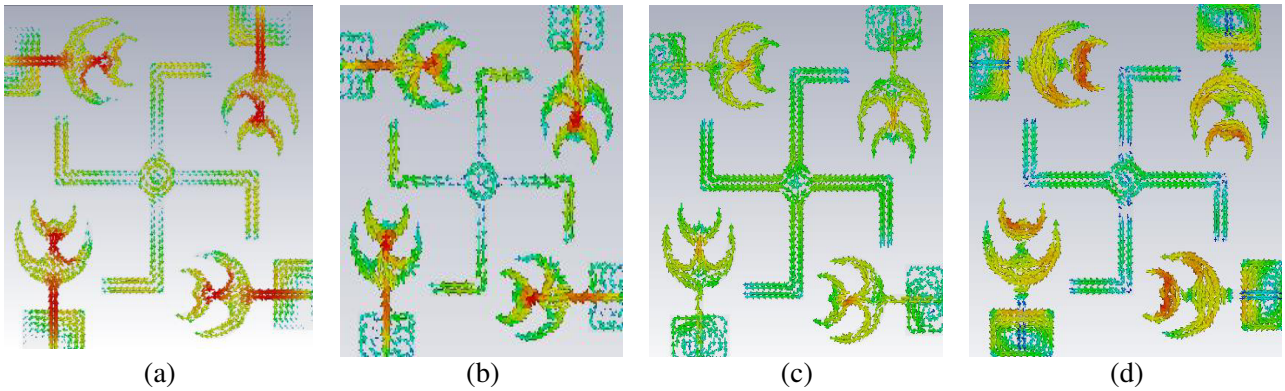

Figure 9. The characteristic currents of CM3 in A#3 at (a) 2.8 GHz, (b) 4.1 GHz, (c) 6.2 GHz, and (d) 8.6 GHz.

3. RESULTS OF FLOWER SHAPED 4 × 4 UWB-MIMO ANTENNA

The performance of a MIMO antenna is primarily determined by its metrics, radiation characteristics, and element isolation. Fig. 11 depicts the designed antenna prototype. The IBW of the flower-shaped

antenna is 10.8 GHz, which falls between 3.1 GHz and 14 GHz, including the ITU band, as shown in Fig. 12. In the UWB spectrum, it also provides good port isolation of −18 dB, as shown in Fig. 13(a).

This antenna covers not only the UWB spectrum, but also the ITU spectrum. At $S_{11} < -10$ dB and in Fig. 12(b), the simulated return losses (S_{11}) are compared to measured values. The vector network analyzer is used to verify the simulation results (VNA).

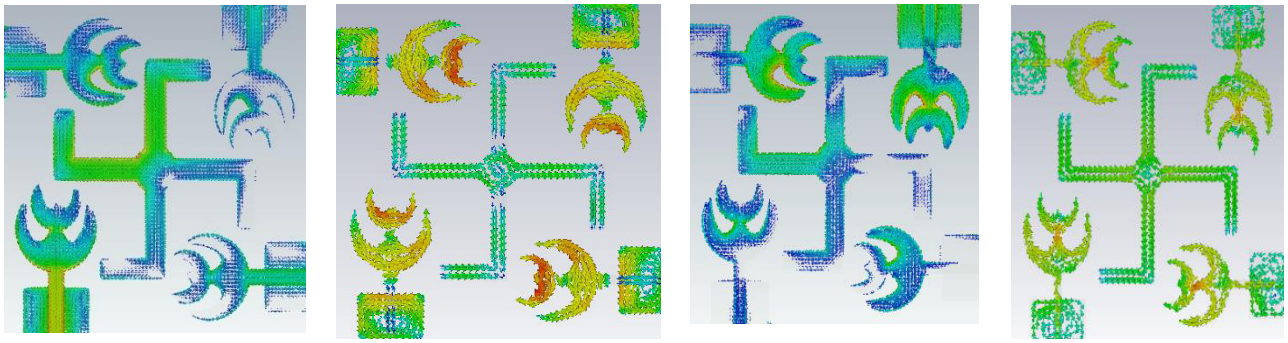

(a) (b) (c) (d)

Figure 10. The current densities in A#3 at (a) 2.8 GHz, (b) 4.1 GHz, (c) 6.2 GHz, (d) 8.6 GHz.

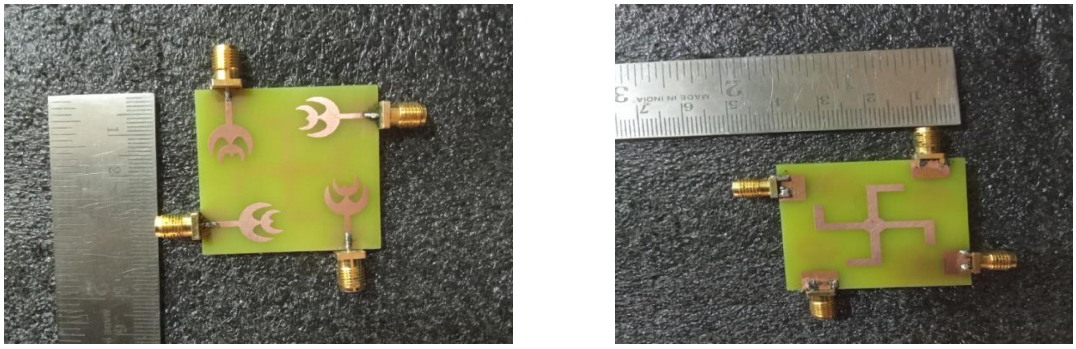

(a) (b)

Figure 11. The proposed flower shaped 4 × 4 UWB-MIMO fabricated antenna. (a) Front View. (b) Back View.

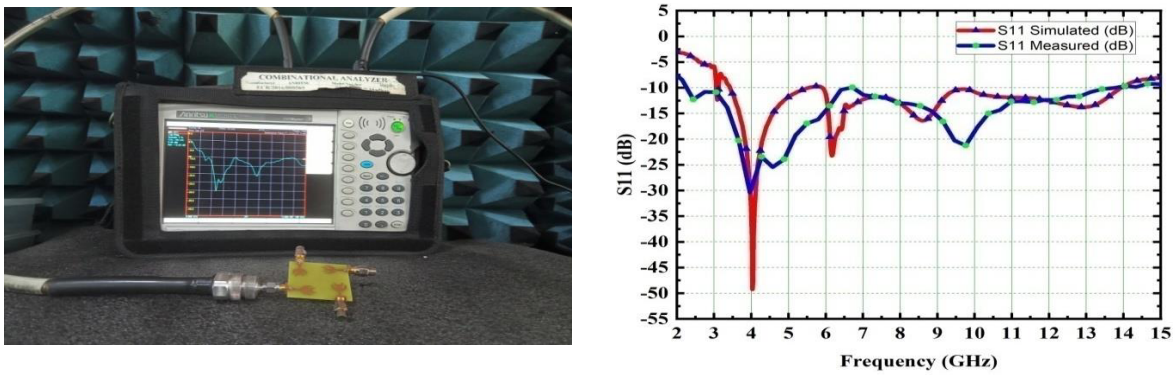

(a) (b)

Figure 12. (a) S_{11} measured. (b) S_{11} measured with simulated.

3.1. Radiation Performance

For radiation patterns the flower-shaped antenna is placed in an anechoic chamber and depicted in Fig. 13(b). At 4.1 GHz, 6.2 GHz, and 8.6 GHz, the co-polarization and cross-polarization patterns are shown in Fig. 14. The radiation patterns are depicted in Fig. 14, which are nearly constant throughout the operating frequency range. The radiation patterns are measured by exciting port 1 and matching port 2 with a matched load. The procedure for the remaining ports 2, 3, and 4 is the same. In Fig. 15, the radiation efficiency and realized gain are 90% and 5.5 dB, respectively.

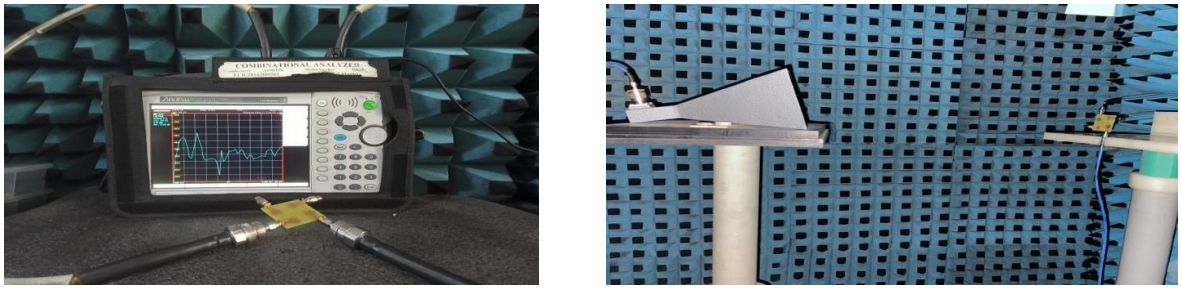

(a) (b)

Figure 13. (a) S_{21} measured. (b) Measurement of radiation pattern in anechoic chamber.

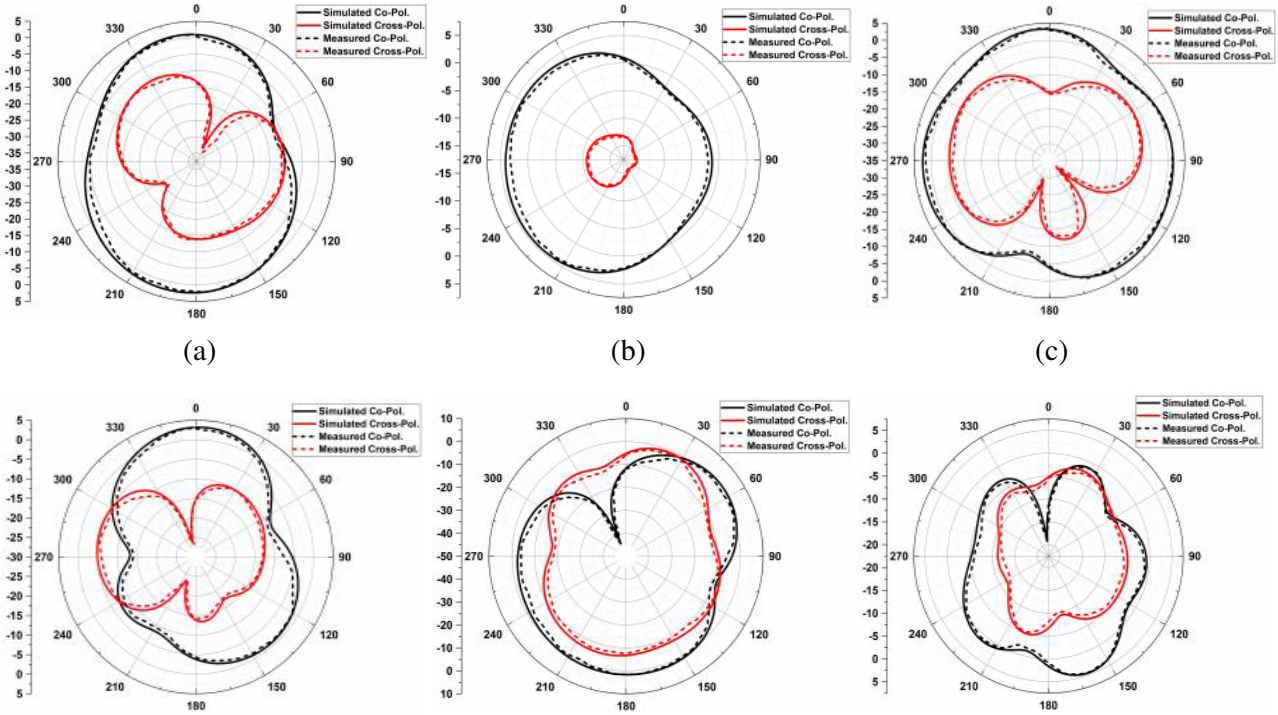

Figure 14. The flower shaped 4×4 antenna radiation pattern of E-Plane at (a) 4.1 GHz, (c) 6.2 GHz, (e) 8.6 GHz and H-plane at (b) 4.1 GHz, (d) 6.2 GHz, (f) 8.6 GHz.

Exciting port 1 and matching the remaining ports with a 50 Ohm load yields the gain. At 4.1 GHz, this antenna performs admirably. This antenna is also ideal for WLAN use. To calculate efficiency, the wheeler cap method is used. The simulated results are compared to the measured efficiency. Because of feeder loss, the measured efficiency differs slightly from the simulated result.

3.2. Diversity Performance

The diversity performance measures are used to see if the designed antenna meets the UWB spectrum's wireless connectivity link requirements. The envelope correlation coefficient (ECC), diversity gain (DG), and mean effective gain (MEG) are examined in the following subsections [30–32].

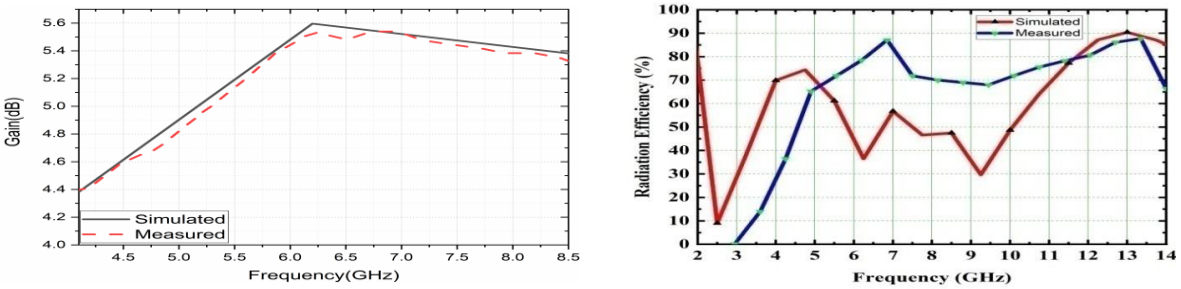

(a) (b)

Figure 15. (a) Comparison of gain simulated with measured. (b) Radiation efficiency.

3.2.1. Envelope Correlation Coefficient (ECC)

One of the important diversity parameters, called the ECC, determines the channel isolation in a wireless communication link. The ECC [30] can be computed using S-parameters or far-fields.

$$\text{ECC} = \frac{\left|S_{kk}^{*}S_{km} + S_{mk}^{*}S_{mm}\right|^{2}}{\left(1-\left(\left|S_{kk}\right|^{2}+\left|S_{mk}\right|^{2}\right)\right)\left(1-\left(\left|S_{mm}\right|^{2}+\left|S_{km}\right|^{2}\right)\right)} \tag{1}$$

$k = 1$ and $m = 2$. The ECC for a lossless or ideal antenna should be zero. In practice, it is not zero and is approaching zero. An appropriate ECC value for a MIMO system is 0.5. In wireless communication, all MIMO antennas should maintain a minimum of 0.5 for reliable communication links. The ECC of the antenna was less than 0.012. Fig. 16(b) depicts the ECC. Because it only has two elements, Equation (1) is suitable for determining ECC in MIMO. When there are more than two antenna elements in a MIMO system, ECC [31] can also be determined by using far fields.

$$\rho_{ij} = \frac{\left|\iint_{4\pi}\left[F_i(\theta,\Phi)\cdot F_j^{*}(\theta,\Phi)\right]\right|^{2}}{\left|\iint_{4\pi}\left|E_i(\theta,\Phi)\right|^{2}d\Omega\cdot\iint_{4\pi}\left|E_j(\theta,\Phi)\right|^{2}d\Omega\right|} \tag{2}$$

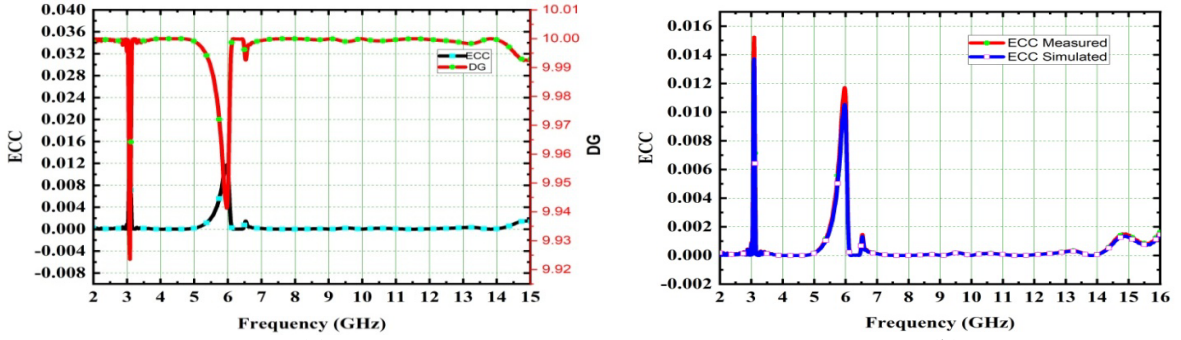

(a) (b)

Figure 16. (a) ECC with DG. (b) ECC.

where $F_i(\theta, \Phi)$ represents the vector field from the ith element; $*$ indicates the complex; and $\cdot$ represents the Hermitian products, respectively. DG is also one of the diversity parameters to describe the communication link reliability in a MIMO system. In ideal MIMO systems, the diversity gain should be nearly equal to 10 dB. The designed antenna achieved 9.998 dB with the help of CMA. The DG is also derived from the ECC. The DG [30] is depicted in Fig. 16(a).

$$DG = 10\sqrt{1 - \text{ECC}^2} \tag{3}$$

3.2.2. Mean Effective Gain

In MIMO systems, the MEG [32] is defined and expressed as

$$\text{MEG}_i = \int_0^{2\pi} \int_0^{\pi} \left[\frac{\acute{\Gamma}}{1+\acute{\Gamma}} G_\theta(\theta, \Phi) P_\theta(\theta, \Phi) + \frac{\acute{\Gamma}}{1+\acute{\Gamma}} G_\Phi(\theta, \Phi) P_\Phi(\theta, \Phi) \right] \sin\theta d\theta d\Phi \tag{4}$$

where $\acute{\Gamma}$ is the cross-polarization discrimination (XPD) of the incident field. The gain pattern components are represented as G_θ and G_Φ for the ith element. The MEG of designed antenna is -3.1 dB and depicted in Fig. 17(a).

3.2.3. CCL (Channel Capacity Loss)

In a MIMO antenna system, the CCL is also an important metric for determining diversity performance. CCL in a MIMO system must be below 0.4 bits/s/Hz to be considered acceptable. The measured and

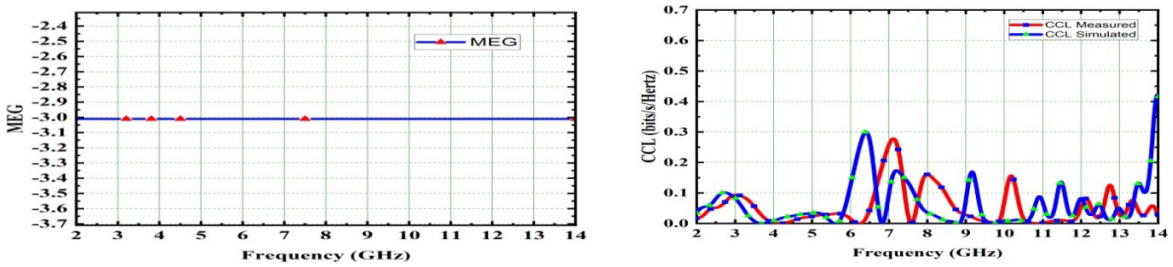

(a) (b)

Figure 17. (a) MEG. (b) CCL.

Table 2. Comparison of the flower shaped UWB MIMO antenna with other models.

S. No.	Ref.	Dimensions (mm^2)	BW (GHz)	Isolation (dB)	Gain (dBi)	ECC	Radiation efficiency (%)
1	[4]	47×93	3.1–10.6	< -20	3.5	—	> 70
2	[5]	50×35	1.9–20	< -22	—	0.003	> 93
3	[6]	40×40	3–11	< -17	< 2	—	> 75.4
4	[11]	40×37.5	2–11	< -20	—	0.1	—
6	[13]	48×34	3.5–10.08	< -23	2.8	< 0.039	> 75
7	[14]	80×50	4.18–6.58	< -17	4	0.056	> 80
8	[15]	45×45	2.2–6.28	< -14	3	< 0.25	> 65
9	[16]	40×40	3.1–11	< -20	3	< 0.004	—
10	[17]	40×40	3–12	< -17	2.9	< 0.06	—
11	[7]	64×45	3.3–7.9	—	3	< 0.02	—
12	[24]	40×40	3–13.5	< -15	3.5	< 0.4	> 89
13	Prop	40×40	3.3–13.75	< -18	5.5	< 0.012	> 89

simulated values of CCL are shown in Fig. 17(b). Throughout the entire frequency spectrum, the proposed antenna achieves a CCL of 0.299 bits/s/Hz.

4. COMPARISONS WITH EXISTING MODELS

The designed antenna shares some similarities and advantages with those previously reported in the literature [4–7, 11–17, 24] and illustrated in Table 2. The designed antenna has the advantage of novelty design compared to other existing models. The proposed antenna with respect to gain, envelop correlation coefficient, impedance bandwidth, and performance of diversity parameters is found to be highly remarkable.

5. CONCLUSIONS

A compact flower-shaped UWB-MIMO antenna is designed with the CMA method. The design application of the flower shape provides miniaturization and offers a good wide band. The flower shape is designed with sepals, and the absence of petals provides good isolation of less than −18 dB in the entire UWB spectrum. This antenna not only covers the UWB spectrum (3.1 GHz–10.6 GHz), but also covers the ITU band (10.7 to 11.7 GHz) and 13 GHz (12.75 to 13.25 GHz). This antenna offers good impedance bandwidth from 3.1 GHz to 14 GHz with good isolation. The radiation characteristics are that radiation efficiency is 90%; bandwidth is 123%; and gain is 5.5 dB. The diversity characteristics of ECC, DG, MEG, and CCL are 0.012, 9.998, −3.1 dB, and 0.29 bits/s/Hz, respectively. This antenna is well suited for WLAN applications. These results are validated in a state-of-art laboratory.

DECLARATION OF COMPETING INTEREST

The authors declare that they have no known competing financial interests or personal relationships that could have appeared to influence the work reported in this paper.

REFERENCES

1. FCC. Washington, DC., "FCC 1st report and order on ultra-wideband technology," FCC, February 2002.
2. Kaiser, T., F. Zheng, and E. Dimitrov, "An overview of ultra-wide-band systems with MIMO," *Proc. IEEE*, Vol. 97, 285–312, 2009.
3. Jiang, C. and L. J. Cimini, "Antenna selection for energy-efficient MIMO transmission," *IEEE Wireless Commun. Lett.*, Vol. 1, No. 6, 577–580, 2012.
4. Radhi, A. H., R. Nilavalan, Y. Wang, H. S. Al-Raweshidy, A. A. Eltokhy, and N. Ab Aziz, "Mutual coupling reduction with a wideband planar decoupling structure for UWB-MIMO antennas," *Int. J. Microwave Wireless Technol.*, Vol. 10, No. 10, 1–12, 2018.
5. Chithradevi, R. and B. S. Sreeja, "A compact UWB MIMO antenna with high isolation and low correlation for wireless applications," *2017 IEEE International Conference on Antenna Innovations & Modern Technologies for Ground, Aircraft and Satellite Applications (iAIM)*, 1–4, Banglore, India, Nov. 24–26, 2017.
6. Mao, C.-X. and Q.-X. Chu, "Compact coradiator UWB-MIMO antenna with dual polarization," *IEEE Trans. Antennas Propagation*, Vol. 62, No. 9, 4474–4480, 2014.
7. Naveen, J., G. S. Dev, T. Ekta, K. Dinesh, K. B. Kumar, and S. Shweta, "Triple band notched mushroom and uniplanar EBG structures based UWB MIMO/diversity antenna with enhanced wide band isolation," *AEU — International Journal of Electronics and Communications*, Vol. 90, 36–44, 2018.
8. Iftikhar, A., B. D. Braaten, and D. E. Anagnostou, "An eight element, compact UWB-MIMO antenna with WLAN band rejection capabilities for 3G/4G/5G communications," *IEEE Open J. Antennas Propagation*, Vol. 1, 196–206, 2020.

9. Iftikhar, A., S. M. Asif, and B. D. Braaten, and D. E. Anagnostou, "Ultra-compact reconfigurable band reject UWB MIMO antenna with four radiator. MDPI," *Electronics*, Vol. 9, 1–9, 2020.
10. Khan, M. S., F. Rigobello, B. Ijaz, E. Autizi, A. D. Capobianco, R. M. Shubair, et al., "Compact 3-D eight elements UWB-MIMO array," *Microwave Opt. Technol. Lett.*, Vol. 60, No. 8, 1967–1971, 2018.
11. Jafri, S. I., R. Saleem, M. F. Shafique, and A. K. Brown, "Compact reconfigurable multiple-input-multiple-output antenna for ultra wideband applications," *IET Microwave Antennas & Propagation*, Vol. 10, No. 4, 413–419, 2015.
12. Nikam, B. V. and M. R. Jadhav, "A compact quad port band-notched MIMO antenna for Wi-Max applications with low mutual coupling," *Progress In Electromagnetics Research C*, Vol. 104, 53–67, 2020.
13. Tiwari, R. N., P. Singh, B. K. Kanaujia, and K. Srivastava, "Neutralization technique based two and four port high isolation MIMO antennas for UWB communication," *AEU — International Journal of Electronics and Communications*, Vol. 110, 152828, 2019.
14. Jehangir, S. S. and M. S. Sharawi, "A miniaturized UWB biplanar Yagi-like MIMO antenna system," *IEEE Antennas Wireless Propagation Lett.*, Vol. 16, 2320–2323, 2017.
15. Anitha, R., P. V. Vinesh, K. C. Prakash, P. Mohanan, and K. Vasudev, "A compact quad element slotted ground wideband antenna for MIMO applications," *IEEE Trans. Antennas Propagation*, Vol. 64, No. 10, 4550–4553, 2016.
16. Wae, A. and A. A. Ibrahim, "A compact double-sided MIMO antenna with an improved isolation for UWB applications," *AEU — International Journal of Electronics and Communications*, Vol. 82, 7–13, 2017.
17. Raikumar, S., A. Amala, and K. T. Selvan, "Isolation improvement of UWB MIMO antenna utilizing molecule fractal structure," *IET Electronic Lett.*, Vol. 10, 576–579, 2019.
18. Iqbal, A., O. A. Saraereh, A. W. Ahmad, and S. Bashir, "Mutual coupling reduction using F shaped stubs in UWB-MIMO antenna," *IEEE Access*, Vol. 6, 2755–2759, 2017.
19. Khan, M. S., A. Iftikhar, S. Asif, A. D. Capobianco, and B. D. Braaten, "A compact four elements UWB MIMO antenna with on-demand WLAN rejection," *Microwave Opt. Technol. Lett.*, Vol. 58, 270–276, 2016.
20. Medkour, H., S. lakrit, S. Das, B. T. P. Madhav, and K. VasuBabu, "A compact printed UWB MIMO antenna with electronically reconfigurable WLAN band-notched characteristics," *Journal of Circuits, Systems and Computers*, 2250045, 2021.
21. Khan, M. S., N. Aftab, A. Iftikhar, R. M. Shubair, S. Asif, and F. Adnan, "A WLAN band-notched compact four element UWB MIMO antenna," *International Journal of RF and Microwave Computer-Aided Engineering*, 1–10, 2020.
22. Babu, K. V. and B. Anuradha, "Design of inverted L-shape & ohm symbol inserted MIMO antenna to reduce the mutual coupling," *AEU — International Journal of Electronics and Communications*, Vol. 105, 42–53, 2019.
23. Saxena, G., Y. K. Awasthi, and P. Jain, "Design of metasurface absorber for low RCS and high isolation MIMO antenna for radio location & navigation," *AEU — International Journal of Electronics and Communications*, Vol. 133, 153680, 2021.
24. han, A. A., S. A. Naqvi, M. S. Khan, and B. Ijaz, "Quad port miniaturized MIMO antenna for UWB 11 GHz and 13 GHz frequency bands," *AEU — International Journal of Electronics and Communications*, Vol. 131, 153618, 2021.
25. Jabire, A. H., H.-X. Zheng, A. Abdu, and Z. Song, "Characteristic mode analysis and design of wide band MIMO antenna consisting of metamaterial unit cell," *Electronics*, Vol. 8, 68, 2019, https://doi.org/10.3390/electronics8010068.
26. Suresh, A. C. and T. S. Reddy, "High isolation with fork-shaped stub in compact UWB-MIMO antenna using CMA," *2021 International Conference on Recent Trends on Electronics, Information, Communication & Technology (RTEICT)*, 505–511, 2021, doi: 10.1109/RTEICT52294.2021.9574028.

27. Singh, H. V. and S. Tripathi, "Compact UWB MIMO antenna with Fork-shaped stub with vias based coupling current steering (VBCCS) to enhance isolation using CMA," *AEU — International Journal of Electronics and Communications*, Vol. 129, 153550, 2021.
28. Barzegari, S., K. Forooraghi, and B. Abbasi Arand, "Design of circularly polarized planar leaky-wave antenna using characteristic mode analysis," *IET Microwaves, Antennas & Propagation*, Vol. 15, No. 9, 1086–1099, 2021.
29. Kumar, N. and R. Khanna, "A compact multi-band multi-input multi-output antenna for 4G/5G and IoT devices using theory of characteristic modes," *International Journal of RF and Microwave Computer-Aided Engineering*, Vol. 30, No. 1, e22012, 2020.
30. Sultan, K. S. and H. H. Abdullah, "Planar UWB MIMO-diversity antenna with dual notch characteristics," *Progress In Electromagnetics Research C*, Vol. 93, 119–129, 2019.
31. Balaji, V. R., T. Addepalli, A. Desai, A. Nella, and T. K. Nguyen, "An inverted L-strip loaded ground with hollow semi-hexagonal four-element polarization diversity UWB-MIMO antenna," *Transactions on Emerging Telecommunications Technologies*, Vol. 33, No. 1, e4381, 2022.
32. Farahani, M. and S. Mohammad-Ali-Nezhad, "A novel UWB printed monopole MIMO antenna with non-uniform transmission line using nonlinear model predictive," *Engineering Science and Technology, an International Journal*, Vol. 23, No. 6, 1385–1396, 2020.